Journal of Biomedical Optics

SPIEDigitalLibrary.org/jbo

Monte Carlo simulation of light transport in tissue for optimizing light delivery in photoacoustic imaging of the sentinel lymph node

Vijitha Periyasamy
Manojit Pramanik

SPIE

Monte Carlo simulation of light transport in tissue for optimizing light delivery in photoacoustic imaging of the sentinel lymph node

Vijitha Periyasamy and Manojit Pramanik
Indian Institute of Science, Electrical Engineering, Biomedical Imaging Laboratory, Bangalore 560012, India

Abstract. Noninvasive or minimally invasive identification of sentinel lymph node (SLN) is essential to reduce the surgical effects of SLN biopsy. Photoacoustic (PA) imaging of SLN in animal models has shown its promise for clinical use in the future. Here, we present a Monte Carlo simulation for light transport in the SLN for various light delivery configurations with a clinical ultrasound probe. Our simulation assumes a realistic tissue layer model and also can handle the transmission/reflectance at SLN-tissue boundary due to the mismatch of refractive index. Various light incidence angles show that for deeply situated SLNs the maximum absorption of light in the SLN is for normal incidence. We also show that if a part of the diffused reflected photons is reflected back into the skin using a reflector, the absorption of light in the SLN can be increased significantly to enhance the PA signal. © *2013 Society of Photo-Optical Instrumentation Engineers (SPIE)* [DOI: 10.1117/1.JBO.18.10.106008]

Keywords: sentinel lymph node; photoacoustic imaging; Monte Carlo simulation.

Paper 130371RR received May 25, 2013; revised manuscript received Sep. 13, 2013; accepted for publication Sep. 23, 2013; published online Oct. 9, 2013.

1 Introduction

National Cancer Institute at the National Institutes of Health defines sentinel lymph node (SLN) as the first lymph node to which cancer cells are most likely to spread from the primary tumor. Sentinel lymph node biopsy (SLNB) can be used to determine the extent or stage of cancer.[1] Surgical effects of SLNB are less compared to axillary lymph node dissection (ALND) in case of breast cancer according to group trails. Only 3% of the patients undergoing SLNB experience wound infections, whereas it affects 8% of the patients undergoing ALND. Quality of life is better in breast cancer patients undergoing only SLNB because there is deterioration of arm movement when ALND is done. However, SLNB is associated with complications like axillary seroma, axillary paraesthesia, lymphedema, sensory nerve injury, limitation in range of motion, and brachial plexus.[1–10] An noninvasive or minimally invasive identification of SLN not only reduces the complications associated with the SLNB, but also opens a new paradigm of molecular imaging through targeted molecular contrast agents.

Photoacoustic (PA) imaging,[11–14] an emerging hybrid imaging modality, combining both optics as well as ultrasound, has been extensively used for SLN mapping of the breast cancer in animal models both using FDA approved methylene blue dye and also several nanoparticles.[15–17] In practice, for SLN imaging, 1% solution of methylene blue dye is injected intradermally at the proximity of breast tumor. This blue colored dye is drained into the primary lymph node by the lymphatic channels. Since PA imaging is capable of giving optical contrast with ultrasound resolution, when tissue is irradiated with a suitable wavelength of light (light wavelength at which methylene blue is strongly absorbing), light travels inside the tissue surface and it is absorbed by the methylene blue dye present in the SLN. Absorbed light energy produces local temperature rise and, due to thermoelastic expansion, acoustic waves are produced, also known as PA waves, which are received by an ultrasonic detector placed on the tissue surface. These recorded PA waves are used to form images of the SLN. The PA waves produced are proportional to the absorbed optical energy in the SLN, which in turn is proportional to the absorption coefficient of the SLN and the light fluence inside the SLN. Since the methylene blue dye has peak absorption around 670 nm, light of this wavelength (or nearby wavelengths) is used to maximize the light absorption in the SLN, and therefore, the generated PA signal is also maximized. The absorption coefficient of methylene blue dye is 10 times stronger than that of the surrounding tissue at this wavelength of light as seen in Table 1. At 664-nm wavelength of light absorption of methylene blue dye is 10 times >95% oxygenated hemoglobin on a per molar basis. More than 146 times contrast has been reported for the SLN images with respect to the surrounding tissue.[17] The amount of light absorption by dye filled SLN will depend on the light delivery geometry and tissue properties surrounding the SLN.

To make PA identification of SLN clinically viable, ultrasonic transducer arrays are used for real-time imaging of the axillary area.[18] In this work, we used a realistic human breast axillary tissue model to simulate how light absorption inside the SLN varies for different configurations of light delivery with a linear ultrasound array receiver probe. It is intuitive to think that irradiating light close to SLN will maximize the light absorption inside the SLN. We validated the intuition using simulations in the first part of the study. Monte Carlo simulation of light transport in multilayered turbid medium (MCML)[19] by

Address all correspondence to: Manojit Pramanik, Indian Institute of Science, Electrical Engineering, Biomedical Imaging Laboratory, Bangalore 560012, India. Tel: +91-80-2293-2372; Fax: +91-80-2360-0444; E-mail: manojit@ee.iisc.ernet.in

0091-3286/2013/$25.00 © 2013 SPIE

Table 1 Optical properties of various layers used in the simulation model at 664-nm wavelength.

Layer	Refractive index (n)	Absorption coefficient-$\mu_a(\text{cm}^{-1})$	Scattering coefficient-$\mu_s(\text{cm}^{-1})$	g	Thickness (cm)
Water	1.3	–	–	–	–
Skin	1.4	0.2525	254	0.9	0.2
Cutaneous fat	1.4	0.1010	123	0.9	30
Sentinel lymph node (SLN) (with methylene blue)	1.3	1.7049	180	0.9	1 (radius)
Air	1.0	–	–		–

Wang et al. is used as the starting point for our simulations. A modified version of the MCML code was used to incorporate the SLN inside the tissue model, also to take care of the reflection/transmission of photons from the SLN tissue interface due to the refractive index mismatch. Mesh-based Monte Carlo or voxel-based Monte Carlo is computationally intensive and it is used only when application demands an accurate fluence map.[20] Since our application is more of a comparative study between different launch configurations of light and our interest is to find out which configuration gives a relatively higher absorption of light inside the SLN, an absolute fluence map is not essential. Moreover, our geometry is a simple one, which can be handled by MCML modifications very well. Monte Carlo can be used to address refractive index mismatch between an embedded object and the surrounding layer by incorporating the refractive index value parametrically rather than the discretized mesh format as in mesh-based Monte Carlo. Our second part of the simulations validates the angle at which the light has to be launched to get optimum PA signals from SLN. In the literature, there have been reports on use of optical reflectors to enhance the light inside the tissue for better imaging.[21] However, it is used for head imaging. Thus, we wanted to check if such concepts can be used for SLN imaging as well. Design of reflector and reflectivity of the material needed to maximize the signal cannot be obtained without proper simulations. So in the last part of the study, first we checked the change in absorption of light in SLN with an increase in the amount of light getting reflected back (percentage of light which is going out of the tissue surface as diffused reflectance) to the tissue by the reflector. Then, we have included a simple flat reflector design shown for different reflecting materials, for which we will have different ranges of light absorption inside the SLN.

These kinds of simulations will be very useful to design a light delivery scheme for integrated PA and ultrasound probes, which in turn will help the clinical translation of PA imaging.

2 Simulation Setup

In humans, the lymph nodes lie at a depth of 0.5 to 3 cm under the skin surface. The average size of the lymph node is also around 1 cm in diameter. In all our simulations, a realistic tissue model with the lymph node embedded at various depths were considered. SLN was embedded in the subcutaneous tissue layer. The skin layer thickness was considered as 0.2 cm. The thickness of subcutaneous layer was considered as 30 cm to make it semi-infinitely deep. Light delivery is experimented with respect to the ultrasound probe of dimension 5×2 cm^2 placed right above the SLN along with a reflector of 3 cm around the transducer. However, the reflector is considered only for the last part of the study. Figure 1 shows the schematic diagram of the simulation model. Table 1 shows the optical properties for various layers used for the simulations. The incident light is assumed to be at 664 nm, the absorption peak of methylene blue dye.[22] The launch medium is assumed to be water/ultrasound gel. Scattering coefficient (μ_s) of methylene blue dye is taken as 180 cm^{-1} because the reduced scattering coefficient (μ_s') is a constant 18 for variation in concentration and wavelength of incident light.[23] Absorption coefficient (μ_a) and μ_s of skin (epidermal and dermal) and subcutaneous fat tissue is also taken at 664 nm.[24]

Original MCML code written in C simulates the light propagation in multilayered tissue. Here, a modified MCML was used. Figure 2 shows the modified flowchart of the MCML used in this work. Dimensionless step size is s, total interaction coefficient μ_t is $\mu_a + \mu_s$, d_b is the distance of the photon to the layer boundary and d_{sb} is the distance of the photon to sphere (SLN) boundary. The refractive index mismatch of SLN (filled with methylene blue dye) and surrounding tissue implies there will be reflection/transmission at SLN–tissue interface. To handle this reflection/transmission at the SLN–tissue interface, the distance between the current location of the photon and the sphere boundary is calculated. This is geometrically seen as a

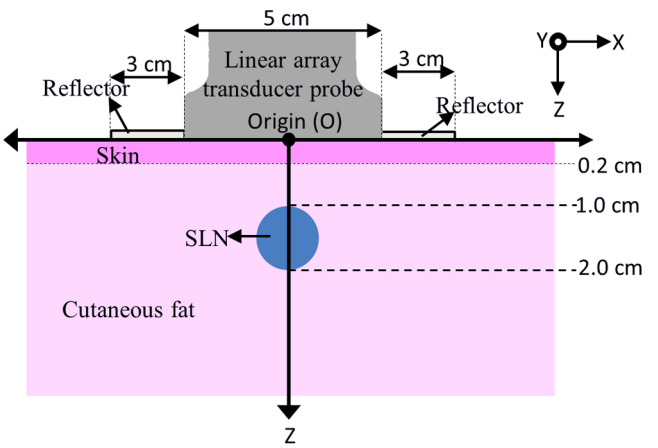

Fig. 1 Schematic diagram of the simulation geometry. Skin layer of thickness 0.2 cm with refractive index (n) = 1.4, $\mu_a = 0.2525$ cm^{-1}, and $\mu_s = 254$ cm^{-1}. Subcutaneous fat of semi-infinite depth with $n = 1.4$, $\mu_a = 0.1010$ cm^{-1}, and $\mu_s = 123$ cm^{-1}. One-cm diameter sentinel lymph node (SLN) placed 1 cm below the skin with $n = 1.3$, $\mu_a = 1.7049$ cm^{-1}, and $\mu_s = 180$ cm^{-1}. $g = 0.9$ for all the layers and SLN. Transducer of 5×2 cm with a reflector of 3 cm around it is positioned on the skin surface ($z = 0$) above the SLN. $n = 1.3$ for water outside the skin.

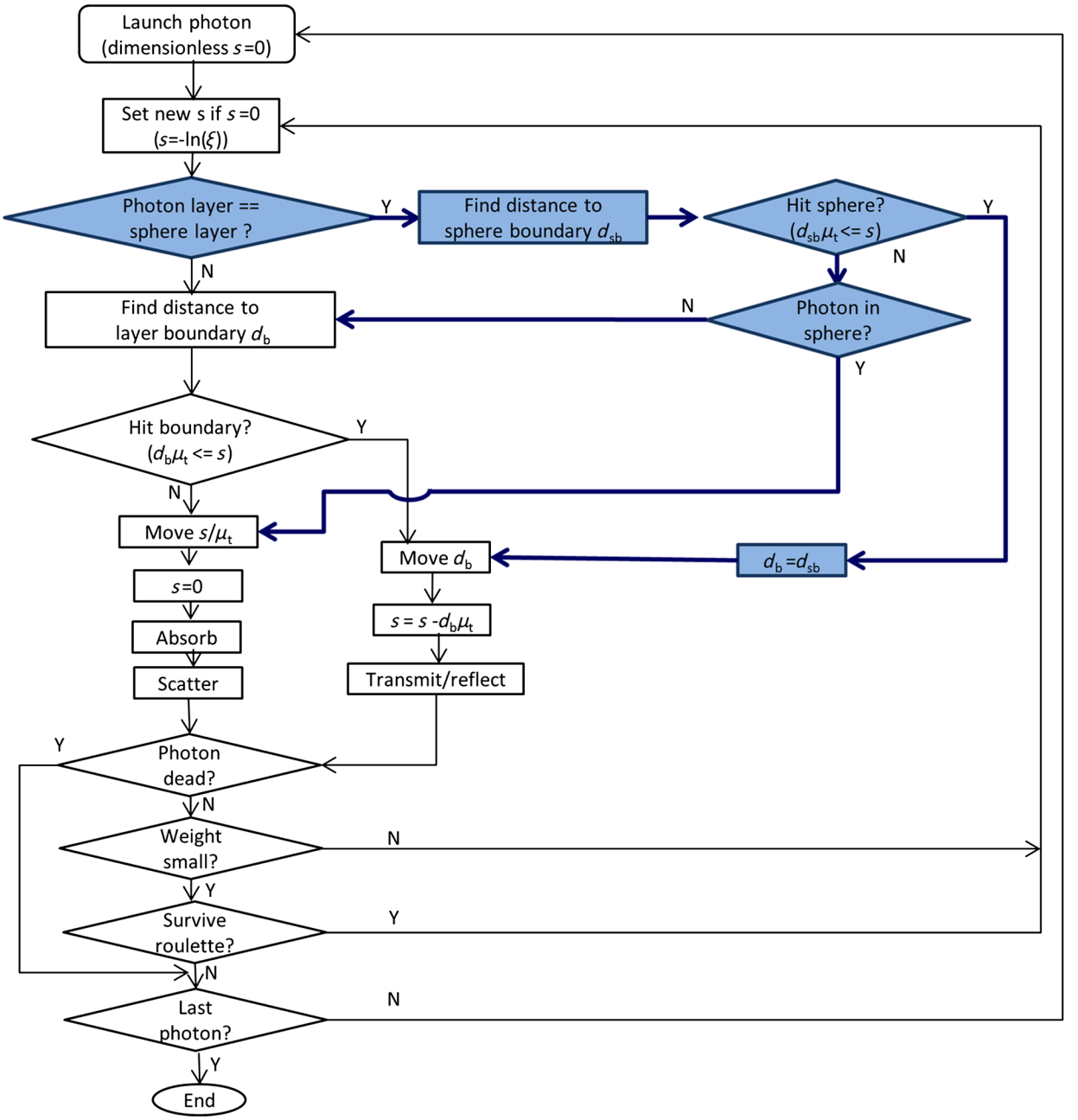

Fig. 2 Modified MCML flow chart for the embedded sphere (SLN). s is the dimensionless step-size, ξ is the random number, d_b is the distance between current location of the photon and the layer, d_{sb} is the distance between current location of the photon and the sphere, and μ_t is the total interaction coefficient.

line intersecting the sphere.[25] If the line intersects the sphere, then direction cosines of the line from photon's current location to the points of intersection is calculated. If the direction cosines match with the direction cosine of the photon's current direction cosine, then the distance between the photon's current location and the point of intersection is calculated. Hit sphere condition is satisfied only if this distance is less than the step size. If the hit sphere is not satisfied, then the photon continues with the boundary check of layers above and below, hop, drop, and spin algorithm as in the original MCML. If the hit sphere condition is satisfied, then the photon is moved to the point of intersection. Then the decision depends on whether the photon is reflected or transmitted on Fresnel's formula. If the photon is transmitted into the SLN, then the weight of the photon is dropped in the next interaction site. Once all the photons are traced, the weight dropped inside the SLN is normalized by the total number of photons to give us the light absorption inside the SLN.

First, various light delivery configurations were designed for a linear array ultrasonic transducer with a foot-print of 5×2 cm^2 as shown in Fig. 3. For the simplicity of the simulation, the light delivery out of the fiber optic is considered as a pencil beam, although a broader beam coming out of multimode fiber can also be simulated.

Case 1: Fiber is right above the SLN on the skin. A hole needs to be drilled inside the ultrasound probe (marked with cross) to realize this light configuration. Thus, this configuration may not be practically feasible. However, for the completeness of the study we have considered this case as well.

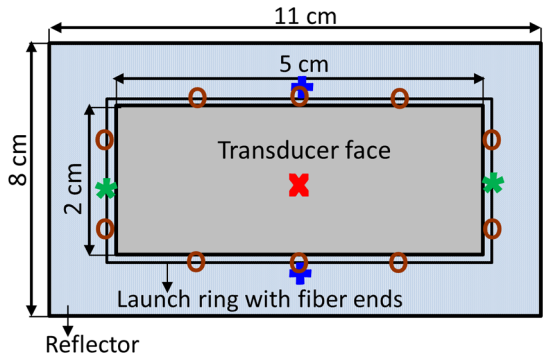

Fig. 3 Transducer with various light delivery configurations. A launch ring is shown to hold the optical fiber to deliver the light on the tissue surface. Case 1: center—Red "X," case 2: shorter side—blue "+," case 3: longer side—green "*," case 4: 10 fibers around transducer—brown "o." A reflector attached around the transducer of 3-cm width.

Case 2: Two optical fibers across the minor axis of the transducer (marked with "+"). Distance between the two light incident locations is 2 cm.

Case 3: Two optical fibers across major axis of the transducer (marked with "*"). Distance between the two light incident locations is 5 cm.

Case 4: Ten fiber cables around the transducer (marked with "o"). Six of them located along the longer sides of the transducer and four of them located along the shorter sides. The locations of the fibers are (−0.8333, 1.0, 0), (0, 1.0, 0), (0.8333, 1.0, 0), (2.5, 0.3333, 0), (2.5, −0.3333, 0), (0.8333, 1.0, 0), (0, −1.0, 0), (0.8333, −1.0, 0), (−2.5, −0.3333, 0) and (−2.5, 0.3333, 0). Units are in cm.

For all the four cases, simulations were run with the SLN placed 1.0 cm below the skin surface. Next, we considered case 2, case 3, and case 4 for various angles in which the fiber can be placed on the skin surface, to see if the launching angle has any effect on the absorption of light inside the SLN situated at various depths under the skin.

Then, we considered a hypothetical situation where the diffused reflected light coming out the skin surface can be reflected back to the skin again by some mechanism. This is to show that diffused light going back to the medium again can increase the light absorption inside the SLN significantly, and thus will improve the signal-to-noise ratio (SNR). For example, the PA enabling device[26] can be modified to reflect back the photons into the tissue to enhance the signal. To model the reflector, the photons that are transmitted out of the skin layer are sent back into the same layer based on the reflectance of the reflector. Since it may not be possible to send back all the photons which are coming back, various percentages of photons are sent back to the skin. When a photon is to be transmitted into skin again, the MCML code with the embedded sphere is modified to increment the diffused reflectance by the weight of the photon multiplied by the (100–percentage of reflected photons)%. The photon with the remaining weight is diverted into the layer with a negation of uz (uz is the direction cosine of the photon with respect to z axis). Since the relaunched photons' location and angle will also depend on the design of the reflector, here, for simplicity, we have assumed that the photons are reflected by a planar mirror where only uz of the photon is negated and there is no other change in the co-ordinates.

Next, we considered a more practical design of a reflector. Photon recycler has been reported earlier for head imaging using PAs. A spherical reflecting surface is used for head imaging, where the PA signals are collected in transmission mode.[21] SLN imaging is done in reflection mode and optical fibers need to be around the transducer. Therefore, we have considered a different kind of reflector. Often the transducers' active surface is covered with thin aluminum foil to minimize transducer generated PA signal when light falls on the transducer. However, the aluminum foil will reduce the sensitivity of the transducer slightly. Since, aluminum foil reflects 90% of the incident light, this itself can be used as a reflector. Moreover, acoustically penetrable optical reflector (APOR) has been reported recently.[27] Thin polyethylene or low-density polyethylene coated with an optically reflecting layer was used to form the APOR whose light reflectivity is reported to be 80%. Acoustic reflection and attenuation is minimal, because acoustic impedance of the APOR is similar to water/ultrasound gel. Therefore, we have repeated the simulations for 90% (aluminum) and 80% (APOR) light reflectivity. The simulations are done for three cases. Case 1: the transducer surface covered with aluminum foil/APOR is considered as the reflecting surface (2×5 cm^2). Case 2: both the transducer surface covered with aluminum foil/APOR as well as the addition reflector around the transducer is considered (8×11 cm^2). Case 3: only the surrounding reflector is considered. This is needed in case we decide to leave the transducer uncovered to retain the acoustic sensitivity. Assuming that the reflecting surface is in contact with the skin surface and under matched boundary conditions, there is no change in the photon path other than the negation of uz for a planar reflector.

In the modified Monte Carlo with the embedded sphere (SLN), the input file is appended with the details of the Cartesian coordinates of sphere center and its radius in centimeter, choice of launch configuration, and the percentage of diffused reflectance going back to the medium. A desktop with i7 Intel 64-bit processor was used for all the simulations.

3 Results and Discussion

Table 2 shows the light absorption within the SLN for all the four light delivery configurations. Each simulation was run with 2 million photons and repeated 10 times. The simulation time is ~587 s (9.78 min) for case 1. It is observed that the absorption of light within the SLN is highest when all the photons are launched from the center of the transducer right above the SLN (case 1). But this configuration may not be feasible to implement, as it may involve modifying the internal structure of the ultrasound transducer itself. Only during the manufacturing of the transducer is such modification feasible. Launch from the fiber across the minor axis (case 2) is the next feasible configuration where absorption of light within the SLN is better than cases 3 and 4. Absorption of light within the SLN for distributed fiber configuration (case 4) is in between that of fiber only across the major axis (case 3) and fiber only across the minor axis (case 2). In case 1, where the light is passed from single fiber cable, there are two problems. First, it needs internal modifications of the transducer array, and second, the fiber's permissible energy limit may not be sufficient to illuminate the tissue surface with the sufficient light energy. [American National Standards Institute (ANSI) safety limit is ~20 mJ/cm^2 for this excitation wavelength.[28]] Hence, there is a need to distribute the light into many fibers as in cases 2–4. Thus, if the incident light can be split into multiple fibers and put across the minor axis of the transducer, one can get the best light absorption

Table 2 Light absorption within the SLN and the diffused reflectance for four different light delivery configurations.

Case	Number of fibers	Position with respect to transducer	Light absorption within the SLN (mean ± SD)	Diffuse reflectance (mean ± SD)
1	1	Center	0.01028 ± 0.00004	0.73235 ± 0.00030
2	2	Across minor axis	0.00390 ± 0.00002	0.73273 ± 0.00022
3	2	Across major axis	0.00017 ± 0.00003	0.73286 ± 0.00020
4	10	Around the transducer	0.00174 ± 0.00002	0.73280 ± 0.00019

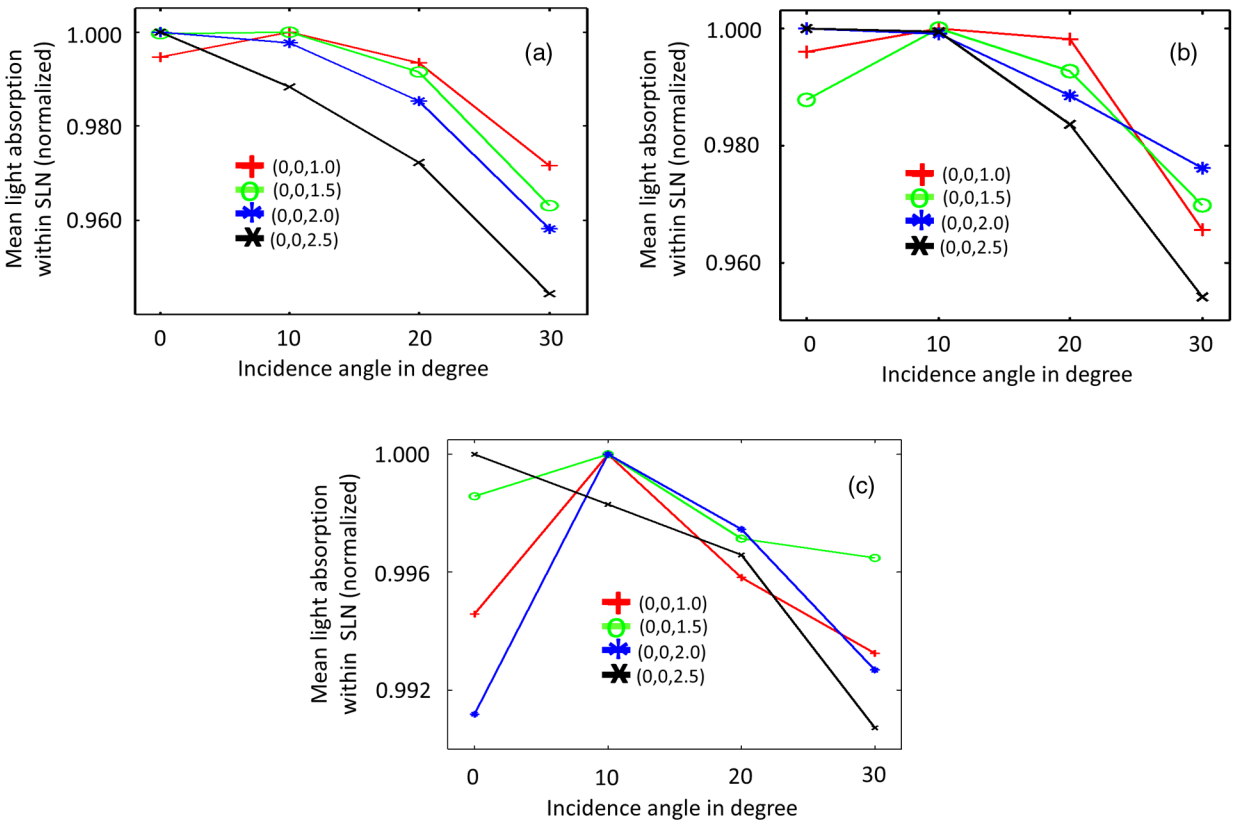

Fig. 4 Mean light absorption within the SLN for four different depths of the SLN. (a) Light delivery through the shorter side of the transducer (case 2), (b) light delivery through the longer side of the transducer (case 3), and (c) light delivery through the fibers distributed around the transducer (case 4).

within the SLN as shown in the simulated results. Although the results obtained here are intuitive to guess that maximum signal could be obtained by illuminating right above the SLN area, the light launching angle also plays a role which cannot be guessed intuitively. In the next section, the effect of various photon launching angles are shown.

Figures 4(a), 4(b), and 4(c) show the normalized mean absorption of light in SLNs centered at 1.0, 1.5, 2.0, and 2.5 cm below the skin surface for various launching angles 0, 10, 20, and 30 deg from the shorter side, longer side, and around the transducer, respectively. It is observed that the absorption of light within the SLN is highest at 10 deg when the SLN is close to the skin surface (1.0 and 1.5 cm under the skin). With the increase in depth of the SLN, launching light perpendicular to the skin gives the highest light absorption within the SLN. Although the change in the light absorption within the SLN is quite small, only ~5% for a 30 deg change in the incident angle, this can be significant when imaging deep

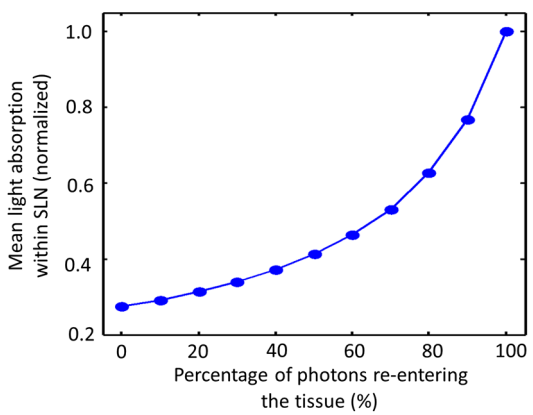

Fig. 5 Normalized light absorption within the SLN for various percentage of diffused reflected light coming out of the skin surface re-entering to the tissue medium. Light delivery configuration 2 and the SLN is placed 1 cm under the skin surface with 10 deg launching angle.

Table 3 Light absorption within the SLN and the percentage of reflected photons re-entering the tissue surface for different reflecting surfaces and reflector types.

		90% reflectivity of the reflector (aluminum)		80% reflectivity of the reflector (APOR)	
Case	Reflecting surface	Light absorption within the SLN (mean ± SD)	Percentage of photons re-entering the tissue (%)	Light absorption within the SLN (mean ± SD)	Percentage of photons re-entering the tissue (%)
1	Transducer covered with reflecting material	0.00739 ± 0.00003	61.41	0.006516 ± 0.00003	52.64
2	Transducer covered with reflecting material and the external reflector	0.01100 ± 0.00002	89.99	0.008961 ± 0.00002	80.00
3	Only external reflector	0.00574 ± 0.00003	55.94	0.005349 ± 0.00002	47.38

SLN where SNR is poor. Similar results are obtained when the fiber is on the longer side of the transducer [case 3, Fig. 4(b)]. Figure 4(c) reveals that there is much less change in the range of normalized mean light absorption within the SLN (0.992—1 or 0.8%). One more difference when compared to case 2 and case 3 is that the SLN centered at 2 cm has maximum absorption of light when the incident light is launched at 10 deg.

Since case 2 gave the best light absorption within the SLN for a feasible light delivery configuration, further simulations were done only for case 2. As observed in Table 2, the diffuse reflected light (light going out of skin surface) is quite significant. The diffused reflected light is 73% and only 0.4% of the light is absorbed within the SLN, which is quite small. Therefore, a smarter design of the PA probe using some mechanism of reflectors, which can send back some portion of the light coming out of the skin back to the medium, is needed. Figure 5 shows an exponential rise in light absorption within the SLN for linear increase in the percentage of light reflected (from the light which is going out of the skin surface) back to the medium again. The launching fiber is placed at 10 deg and the SLN is placed 1 cm below the skin. The light absorption within the SLN increased from 0.4% to 1.4% when 100% of light was redirected to the medium. A significant increase in the light absorption within the SLN can be achieved even with 60% to 80% photons coming back to the medium. At this wavelength of excitation light (664 nm), the ANSI safety limit is ~20 mJ/cm^2.[28] A typical PA system for SLN imaging will use <10 mJ/cm^2 for illumination. For example, a contrast of 24.5 for SLN (at 2 cm under skin) with respect to the background was reported with an illumination of 3.4 mJ/cm^2 at 635 nm.[17] Thus, even if 10 mJ/cm^2 of laser energy is used and 90% of the diffused reflected light is reflected back into the skin, it will still be well within ANSI limits.

Next, simulations were continued for a more practical reflector design. Table 3 shows the results. Just by covering the transducer face with aluminum foil, light absorption within the SLN increased from 0.003 to 0.006–0.007. With a reflector of 3 cm around the transducer, the light absorption within the SLN increased to 0.005–0.006. If photons are reflected from transducer face and the reflector, the light absorption within the SLN increased to 0.009–0.011. The percentage of photons reflected back by the reflecting surface (photons reflected back/photons that were going out of the skin surface) is given in Table 3. We see that 50% to 90% of the photons can be reflected back to the tissue using a reflecting material which has 80% to 90% light reflectivity. Depending on the reflector material properties or the size of the reflector used (in our case 3 cm) the percentage of light sent back to the tissue can be improved. The results show that it is possible to enhance the light absorption inside the SLN, which in turn will enhance the PA signal generation.

4 Conclusion

A modified Monte Carlo simulation is used to see which light delivery configuration maximizes the light absorption inside the SLN in the axillary area for the minimally invasive identification of SLN using PA imaging. Various light delivery configurations are considered around a typical commercial ultrasound array detector probe. Moreover, various launch angles of the photons are considered. Simulations show that, depending on the depth of the SLN, one can change the incident angle to maximize the PA signal from the SLN. Also, when the fiber is placed through the transducer at the center, maximum light absorption within the SLN is achieved. However, due to practical challenges, the next best option is to use the shorter side of the transducer for placing the fibers. It is also shown that with re-use of the diffused reflected light coming out of the skin surface, it is possible to enhance the light absorption within the SLN. For the sake of simplicity, we considered a pencil beam in our simulations. A multimodal fiber can also be considered by launching the photons on a circular area (size of the fiber tip). If the system is spatially invariant, convolution MCML can also be used to reduce computation time. Although the study is not complete for all types of reflector designs, we showed for a very simple reflector design it is possible to enhance the PA signal inside the SLN significantly. Simulations of this nature will help to design the light delivery for optimum PA signal generation and clinical translation of the imaging system.

References

1. "Sentinel lymph node biopsy," http://www.cancer.gov/cancertopics/factsheet/detection/sentinel-node-biopsy (08November2011).
2. "Treatment of early-stage cancer," *JAMA*, **265**(3), 391–395 (1991).
3. K. K. Swenson et al., "Comparison of side effects between sentinel lymph node and axillary lymph node dissection for breast cancer," *Ann. Surg. Oncol.* **9**(8), 745–775 (2002).
4. D. Krag et al., "The sentinel node in breast cancer—a multicenter validation study," *N. Engl. J. Med.* **339**(14), 941–946 (1998).
5. K. M. McMasters et al., "Sentinel lymph node biopsy for breast cancer: a suitable alternative to routine axillary dissection in multi-institutional practice when optimal technique is used," *J. Clin. Oncol.* **18**(13), 2560–2566 (2000).
6. A. D. Purushotham et al., "Morbidity after sentinel lymph node biopsy in primary breast cancer: results from a randomized controlled trial," *J. Clin. Oncol.* **23**(19), 4312–4321 (2005).

7. O. A. Ung et al., "Australasian experience and trials in sentinel lymph node biopsy: The RACS SNAC trial," *Asian J. Surg.* **27**(4), 284–290 (2004).
8. A. Lucci et al., "Surgical complications associated with sentinel lymph node dissection (SLND) plus axillary lymph node dissection compared with SLND alone in the American College of Surgeons Oncology Group Trial Z0011," *J. Clin. Oncol.* **25**(24), 3657–3663 (2007).
9. R. Belmonte et al., "Quality-of-life impact of sentinel lymph node biopsy versus axillary lymph node dissection in breast cancer patients," *Value Health* **15**(6), 907–915 (2012).
10. L. G. Wilke et al., "Surgical complications associated with sentinel lymph node biopsy: results from a prospective international cooperative group trial," *Ann. Surg. Oncol.* **13**(4), 491–500 (2006).
11. L. H. V. Wang and S. Hu, "Photoacoustic tomography: in vivo imaging from organelles to organs," *Science* **335**(6075), 1458–1462 (2012).
12. X. Wang et al., "Noninvasive laser-induced photoacoustic tomography for structural and functional in vivo imaging of the brain," *Nat. Biotechnol.* **21**(7), 803–806 (2003).
13. H. F. Zhang et al., "Functional photoacoustic microscopy for high-resolution and noninvasive in vivo imaging," *Nat. Biotechnol.* **24**(7), 848–851 (2006).
14. C. G. A. Hoelen et al., "Three-dimensional photoacoustic imaging of blood vessels in tissue," *Opt. Lett.* **23**(8), 648–650 (1998).
15. M. Pramanik et al., "In vivo carbon nanotube-enhanced non-invasive photoacoustic mapping of the sentinel lymph node," *Phys. Med. Biol.* **54**(11), 3291–3301 (2009).
16. D. Pan et al., "Near infrared photoacoustic detection of sentinel lymph nodes with gold nanobeacons," *Biomaterials* **31**(14), 4088–4093 (2010).
17. K. H. Song et al., "Noninvasive photoacoustic identification of sentinel lymph nodes containing methylene blue in vivo in a rat model," *J. Biomed. Opt.* **13**(5), 054033 (2008).
18. T. N. Erpelding et al., "Sentinel lymph nodes in the rat: noninvasive photoacoustic and US imaging with a clinical US system," *Radiology* **256**(1), 102–110 (2010).
19. L. H. V. Wang, S. L. Jacques, and L. Zheng, "MCML–Monte Carlo modelling of light transport in multi-layered tissues," *Comput. Methods Programs Biomed.* **47**(2), 131–146 (1995).
20. Q. Fang, "Mesh-based Monte Carlo method using fast ray-tracing in Plücker coordinates," *Biomed. Opt. Express* **1**(1), 165–175 (2010).
21. L. Nie et al., "Photoacoustic tomography through a whole adult human skull with a photon recycler," *J. Biomed. Opt.* **17**(11), 110506 (2012).
22. "Tabulated molar extinction coefficient for methylene blue in water," http://omlc.ogi.edu/spectra/mb/mb-water.html (2011).
23. S. Fantini et al., "Absolute measurement of absorption and scattering coefficients spectra of a multiply scattering medium," *Proc. SPIE* **2131**, 356 (1994).
24. C. R. Simpson et al., "Near-infrared optical properties of ex vivo human skin and subcutaneous tissues measured using the Monte Carlo inversion technique," *Phys. Med. Biol.* **43**(9), 2465–2478 (1998).
25. M. L. Khanna, *Solid Geometry: Co-ordinate Geometry of Three Dimensions*, 17th ed., Jai Prakash Nath Publications, Meerut (1987).
26. L. G. Montilla et al., "Real-time photoacoustic and ultrasound imaging: a simple solution for clinical ultrasound systems with linear arrays," *Phys. Med. Biol.* **58**(1), N1–12 (2013).
27. Z. Deng et al., "Acoustically penetrable optical reflector for photoacoustic tomography," *J. Biomed. Opt.* **18**(7), 70503 (2013).
28. American National Standards Institute, "American National Standard for the Safe Use of Lasers," ANSI Z136.1-2000, American National Standards.